Available online at www.sciencedirect.com

SciVerse ScienceDirect

Ceramics International 39 (2013) 7043–7051

CERAMICS INTERNATIONAL

www.elsevier.com/locate/ceramint

Effect of polyethylene glycol on the electrophoretic deposition of hydroxyapatite nanoparticles in isopropanol

Saeede Kuche Loghmani[1], Morteza Farrokhi-Rad[1], Taghi Shahrabi*

Department of Materials Science & Engineering, Tarbiat Modares University, P.O. Box 14115-143, Tehran, Iran

Received 14 August 2012; received in revised form 14 February 2013; accepted 15 February 2013
Available online 21 February 2013

Abstract

The suspensions of hydroxyapatite (HA) nanoparticles were prepared in isopropanol and polyethylene glycol (PEG) was used as a dispersant. The suspensions were characterized by various tests such as electrical conductivity, zeta potential, Fourier transform infrared spectroscopy (FTIR) and particle size distribution. The results showed that PEG is protonated and then adsorbed on the surface of HA nanoparticles enhancing their stability by an electrosteric stabilization mechanism. Electrophoretic deposition (EPD) was performed at different voltages (60 and 200 V) and times (15, 30, 60, 120, 240 and 360 s). EPD from the suspension with 2 g/L PEG showed the fastest kinetic due to the highest zeta potential (+32.9 mV) of HA nanoparticles in it. The wet density of deposits increased with deposition time and voltage due to the particles rearrangement within it during EPD under the influence of electro-osmotic flow. The SEM images showed that the deposit formed from the suspension with 2 g/L PEG had a finer microstructure with less agglomeration. Optical microscope images showed that PEG acted as an effective binder to prevent from deposit cracking during drying. The coating deposited from the suspension with 2 g/L PEG had the best corrosion resistance in Ringer's solution at 37.5 °C.

Keywords: C. Corrosion; Hydroxyapatite (HA) nanoparticles; Electrophoretic deposition (EPD); Polyethylene glycol (PEG); Isopropanol

1. Introduction

Metals are usually used as the orthopedic implants due to their good mechanical properties [1–4]. However, they corrode in contact with body fluid releasing the toxic metallic ions into the surrounding tissues which can damage them [5,6]. In addition to this, metals and their alloys are not bioactive resulting in the poor adhesion of metallic implant to the surrounding tissues [7–9]. Due to corrosion and poor adhesion to living tissues, the surface of metallic implants is usually treated to improve their biocompatibility and bioactivity [10]. Coating the metallic implants with bio-ceramics such as hydroxyapatite (HA) and bioactive glasses induces the growth of natural bone at the interface between implant and tissue [11–13]. HA ($Ca_{10}(PO_4)_6(OH)_2$) is an important material for application in biomedical implants, since its chemical composition is very similar to the inorganic part of bone resulting in its high biocompatibility, bioactivity and ability to bond with bone. However, HA has poor mechanical properties limiting its usage in high load bearing applications. To overcome this problem usually HA is coated on the metallic implants. HA coated metallic implants combine the good mechanical properties of metals and excellent biocompatibility and bioactivity of HA, simultaneously [14–17]. HA have been coated on metallic substrates by several techniques such as sol–gel [18], plasma spraying [19], dip coating [20], plasma sputtering [21] and pulsed laser deposition [22]. Electrophoretic deposition (EPD) is another method that has been used extensively in recent years to deposit HA coatings on metallic substrates [14,17,23–25]. EPD is a two step process: in the first step the charged particles are dispersed in a solvent and move toward the electrode with opposite charge under the influence of an applied electric field; in the second step they deposit and form a relatively dense layer of particles on it [26]. EPD has several advantages such as simplicity, need low cost equipments, ability to control the microstructure of deposit by

*Corresponding author. Tel.: +98 2182883378; fax: +98 2182883381.
E-mail addresses: morteza_farrokhi_rad@yahoo.com (M. Farrokhi-Rad), tshahrabi34@modares.ac.ir (T. Shahrabi).
[1]These authors contributed equally to this work.

0272-8842/$ - see front matter © 2013 Elsevier Ltd and Techna Group S.r.l. All rights reserved.
http://dx.doi.org/10.1016/j.ceramint.2013.02.043

adjusting the deposition parameters (such as voltage and time) and so on [26]. Another unique advantage of the EPD method is its ability to deposit HA coatings with interconnected porosity enhancing the bone ingrowths into the coatings [27]. The kinetics of EPD follows from the equation proposed by Hamaker [28]:

$$\frac{dw}{dt} = \mu cAE \tag{1}$$

In this equation μ is the electrophoretic mobility of particles, c is particles concentration in suspension, A is the deposition area and E is the applied electric field. The electrophoretic mobility of particles can be obtained by the following equation [29]:

$$\mu = \frac{\varepsilon\varepsilon_0\zeta}{\eta} \tag{2}$$

where ζ is the zeta potential of particles, ε_0 is vacuum permittivity, ε_r is the relative dielectric constant of medium and η is the viscosity of medium.

The colloidal stability of particles in the suspension has a great influence on the quality of coatings electrophoretically deposited from it. Due to water electrolysis at relatively low applied electric fields, its usage as the solvent for suspension preparation is limited in EPD [30]; so usually organic mediums such as alcohols are used as the suspension medium in EPD [31]. The surface charge and so the colloidal stability of particles in the non-aqueous solvents is very low. So the addition of dispersants into the non-aqueous suspensions can enhance the zeta potential and colloidal stability of particles in them. Xiao and Liu [17] used triethanolamine as the effective dispersant to prepare the stable suspension of HA nanoparticles in butanol for EPD.

In the present work the effects of polyethylene glycol (PEG) on the properties of HA nanoparticles suspension in isopropanol and their EPD process were investigated.

2. Materials and method

2.1. Suspension preparation

Hydroxyapatite (HA) nanoparticles were synthesized by the wet chemical method [14]. The synthesized nanoparticles were characterized by XRD and SEM analysis. Isopropanol (Merck, 99.8%) and PEG (molecular weight: 4000 g/mol, Merck, reagent grade) were used as the solvent and dispersant (and binder), respectively. For suspensions preparation various concentrations of PEG (1, 2, 4 and 6 g/L) were added into 100 mL of isopropanol and dissolved by stirring them for 15 min. Then 10 g/L of HA nanoparticles were added into them and magnetically stirred for 24 h. Finally the suspensions were ultrasonicated (Sonopulse HD 3200, 20 kHz, Bandelin Co, Germany) for 10 min. The electrical conductivity of the suspensions was measured against PEG concentration using conductivity meter (WTW, inoLab Cond 720, Germany) with the accuracy of ± 0.01 μS/cm before and after the addition of HA nanoparticles. The zeta potential as well as the particle size distribution of HA nanoparticles were measured versus PEG concentration (Malvern instrument). The suspensions for zeta potential measurement were diluted according to the method described in [31]. Fourier transform infrared spectroscopy (FTIR) analysis was performed to investigate the adsorption of PEG on the surface of HA nanoparticles. The samples for FTIR analysis were prepared by removing some powder from the suspension containing 2 g/L PEG (by centrifuging and washing them with deionized water (2 times, at 4000 rpm)) and drying them at 100 °C for 24 h.

2.2. Electrophoretic deposition

A two electrode cell was used for EPD. The plates of 316L stainless steel with the dimension of 2×4 cm^2 were used as the substrates. Only 4 cm^2 of the substrates was exposed to deposition and remainder of their surface insulated. The counter electrode was also a plate from 316 L stainless steel with the same dimension of the substrate. The distance between two electrodes was adjusted in 1 cm. EPD was performed at 60 and 200 V for different times (15, 30, 60, 120, 240 and 360 s). The current density was recorded by computer connected multimeter (Fluke, 289 True RMS) during EPD. The electrical resistance of the deposits ($R_{d,t}$) was calculated against EPD time according to the following equation [31]:

$$R_{d,t} = \frac{V_{app}}{i_t} - R_s \tag{3}$$

where V is the applied voltage and i_t is the current passes through the circuit at any moment. R_s was calculated according to Ohm's equation by dividing the applied voltage by the current passing through the circuit at $t=0$. The effective field over the suspension was calculated according to the following equation [32]:

$$V_{eff,t} = V_{app} - V_{drop,t} \quad \text{and} \quad V_{drop,t} = R_{d,t} i_t \tag{4}$$

where $V_{drop,t}$ is the voltage drop over the deposit at any time.

The wet weight of deposits (W_W) was measured immediately after deposition (GR-200, A&D Co., Tokyo, Japan, accuracy: 0.1 mg) and their immersion weight (W_i) was recorded according to the method described in [32].

The wet density (ρ_W) of the deposits was calculated according to the following equation:

$$\rho_W = \frac{W_W}{V_W} \quad \text{and} \quad V_W = \frac{W_W - W_i}{\rho_{ISP}} \tag{5}$$

where V_W is the wet volume of deposit and ρ_{ISP} is the density of isopropanol (0.78 g cm^{-3}).

The deposits were sintered at 600 °C for 1 h (heating rate: 5 °C/min). The microstructure of deposits was observed by optical and scanning electron microscopy (SEM) before and after sintering.

2.3. Corrosion study

Corrosion resistance of deposits was studied by dynamic polarization analysis (Autolab 84367) in Ringer's solution at 37.5 °C. A three electrode electrochemical cell was used for polarization analysis in which substrate, palatine and saturated calomel electrode (SCE) were acting as working, counter and reference electrode, respectively. Polarization was performed in the potential range of −0.8 to 0.8 V relative to open circuit potential (OCP) at the scan rate of 1 mV/min.

3. Result and discussion

3.1. Synthesized HA nanopowder

The XRD pattern of synthesized nanopowder is shown in Fig. 1. The XRD pattern shows the HA characteristic peaks (according to the standard card of HA: JCPDS 09-432). The SEM image of synthesized powder is shown in Fig. 2. As can be seen the nanoparticles have spherical morphology with the dimension of about 30 nm.

3.2. Effect of PEG on suspension properties

3.2.1. Electrical conductivity

The variation of electrical conductivity of isopropanol in the presence as well as the absence of 10 g/L HA nanoparticles against PEG concentration is shown in Fig. 3. The electrical conductivity of isopropanol as well as suspension increases continuously with PEG concentration. Also the electrical conductivity of suspension is less than that of the solution (PEG in isopropanol) at same PEG concentration. The electrical conductivity of isopropanol increases with PEG addition due to the following reaction:

$$PEG + ROH \rightarrow H^+PEG + RO^- \quad (6)$$

According to Le Chatelier's principle, reaction (6) goes further to the right side when the concentration of PEG increases in isopropanol resulting in further increase in its electrical conductivity. When HA nanoparticles are added into the solution (PEG in isopropanol), H^+PEG species (generated by reaction (6)) are adsorbed on their surfaces

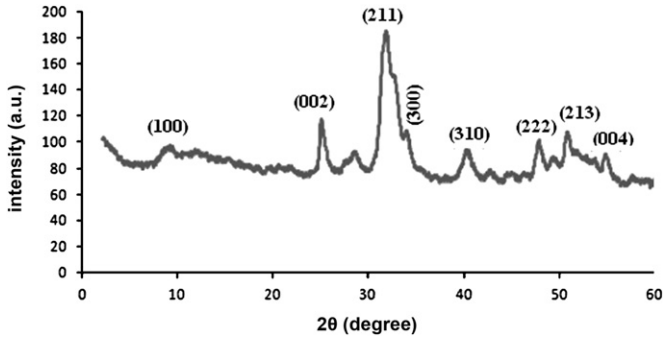

Fig. 1. X-ray diffraction pattern for synthesized HA nanopowder.

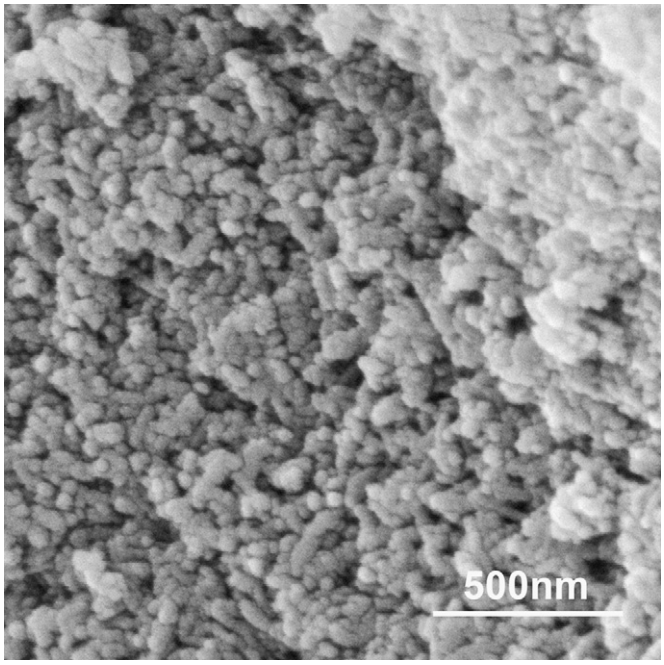

Fig. 2. SEM image of synthesized HA nanopowder.

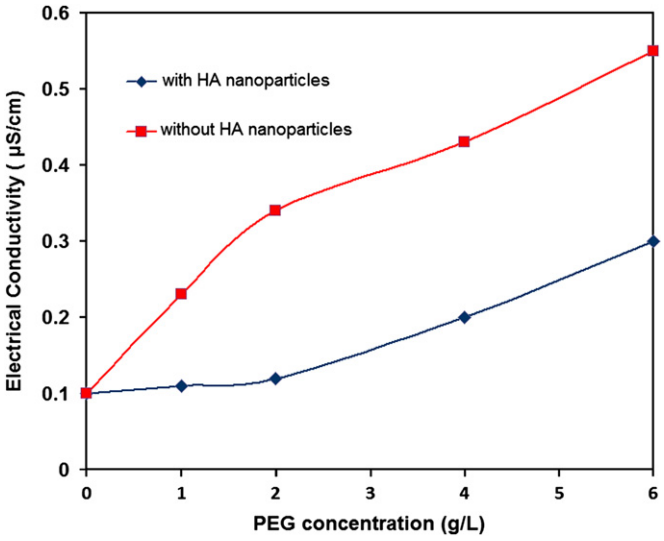

Fig. 3. Electrical conductivity of isopropanol against PEG concentration in the presence and absence of 10 g/L HA nanoparticles.

(as proved by FTIR analysis, Fig. 6) resulting in the conductivity drop (since the mobility of free ions (H^+PEG) is higher than charged particles). Also it can be seen that the conductivity of suspension increases faster when the PEG concentration is more than 2 g/L; this can be due to the saturation of HA nanoparticles by PEG at this concentration.

3.2.2. Zeta potential

The zeta potential of particles against PEG concentrations is shown in Fig. 4. As can be seen in Fig. 4, HA nanoparticles have positive zeta potential in pure isopropanol indicating

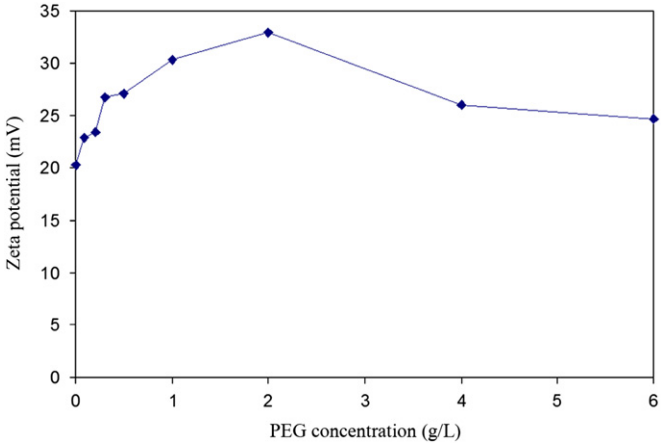

Fig. 4. Zeta potential of HA nanoparticles (10 g/L) against PEG concentrations in isopropanol.

that they acquire positive surface charge in it. According to the mechanism proposed by Damodaran and Moudgil [33] two alcohol molecules are adsorbed on the surface of HA nanoparticles and ionize to yield a protonated alcohol and an alkoxide ion; protonated alcohol dissociate leaving the proton on the HA surface. Then the dissociated alcohol and the alkoxide ion desorb into the solution, resulting in the positively charged HA nanoparticles in pure alcohol. Also as can be seen in Fig. 4, the zeta potential initially increases with PEG concentration and then decreases upon its further addition. When the PEG concentration in the suspensions increases, the concentration of protonated PEG adsorbed on the nanoparticles increases resulting in the increase in zeta potential. The excessive addition of PEG results in some drop in the zeta potential due to the enhancement in the ionic strength of the suspension [34].

3.2.3. Particle size distribution

The particles size distribution of suspensions containing 10 g/L HA with the different concentrations of PEG after 30 days of preparation is shown in Fig. 5. As can be seen, the suspension containing 2 g/L PEG has a finer and narrower particle size distribution than the other suspensions. As it was explained the zeta potential of HA nanoparticles in the suspension with 2 g/L PEG is the maximum (32.9 mV) resulting in their less agglomeration than other suspensions. It must be mentioned that the fraction of particles size appeared in the size range of 4000–5000 nm is due to the air bubble trapped in the suspensions.

3.2.4. PEG adsorption at HA nanoparticles

The results for FTIR analysis are shown in Fig. 6. In addition to the peaks appeared in the spectra of the powder removed from the suspension without PEG, the spectra of that removed from the one with 2 g/L PEG show several other peaks attributed to PEG proving its adsorption on HA nanoparticles. The peaks appeared at 2891, 2737, 2692, 1343 cm^{-1} are attributed to different

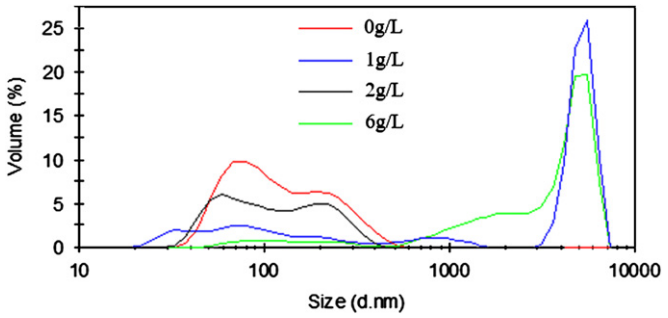

Fig. 5. Particle size distribution for the suspensions containing different concentrations of PEG after 30 days of preparation.

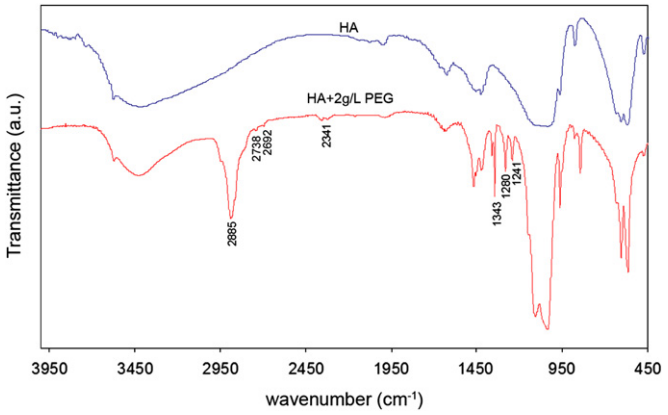

Fig. 6. Results of FTIR analysis for powder removed and dried from the suspensions without and with 2 g/L PEG.

vibration modes of C–H bond of PEG. The peaks at 1283 and 1241 cm^{-1} belong to C–C bond [35,36]. The adsorption of PEG can occur through the hydrogen bonding between the O–H groups of PEG and surface P–OH groups of HA nanoparticles. The adsorption of several chemicals through hydrogen bonding with surface P–OH groups of HA has been reported in the literature [37,38].

3.3. Elecrophoretic deposition

3.3.1. Electrical parameters

Fig. 7 shows variation in current density, the electrical resistance of the deposits and the effective field over the suspension during EPD at 60 and 200 V from the suspensions with different PEG concentrations. The current density and effective field decreases and resistance increases with deposition time for all the suspensions and at both applied voltages due to the deposits thickening with time. The effective field across the suspension during EPD depends on the conductivity of the suspension and the resistivity of the deposit. The different effective fields are present across the suspensions during EPD (Fig. 7c,f) due to different conductivities of the suspensions (Fig. 3) resulting in the different variation from linearity in the kinetics curves (Fig. 8) obtained for the suspensions with various concentrations of PEG. As voltage increases from 60 to 200 V, the

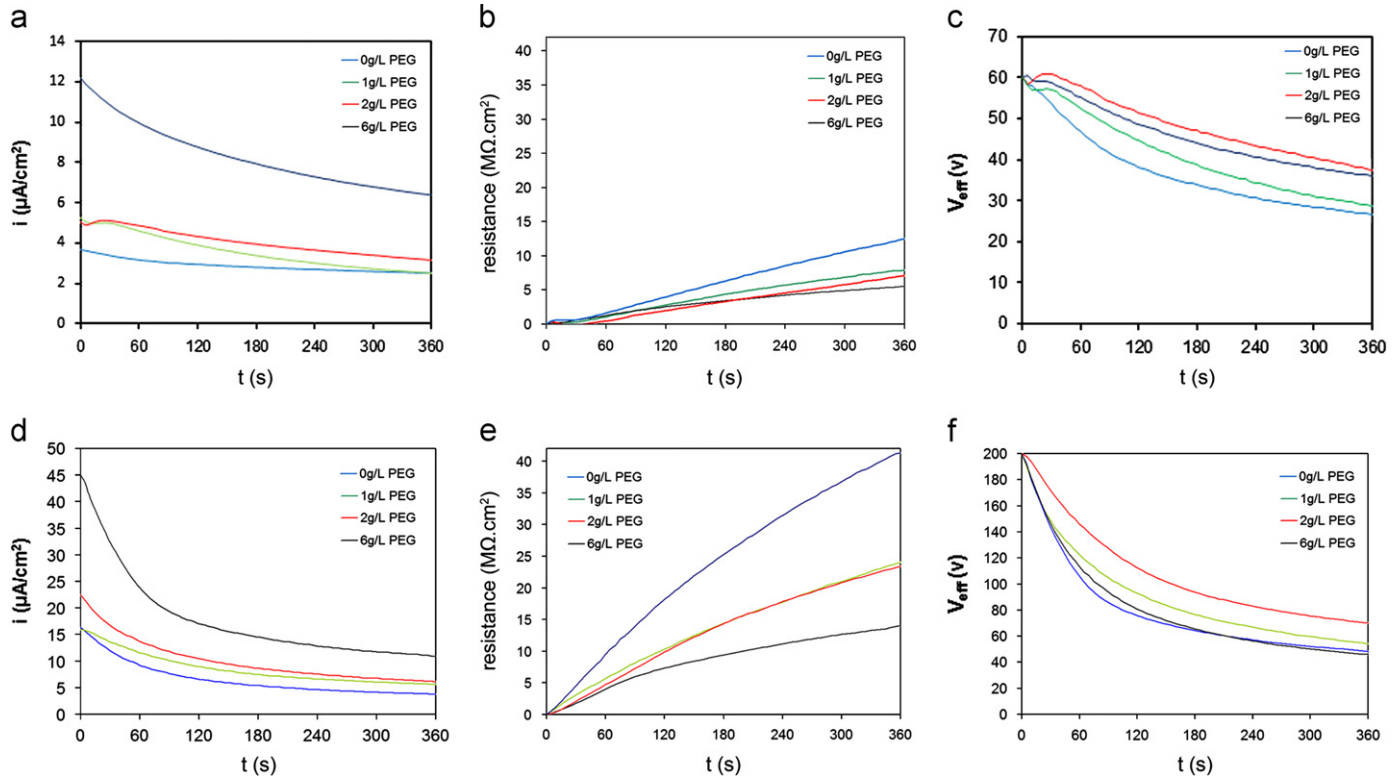

Fig. 7. Current density, electrical resistance of deposits and effective electric field across the suspensions versus EPD time at (a) 60 and (b) 200 V form the suspensions with different concentrations of PEG.

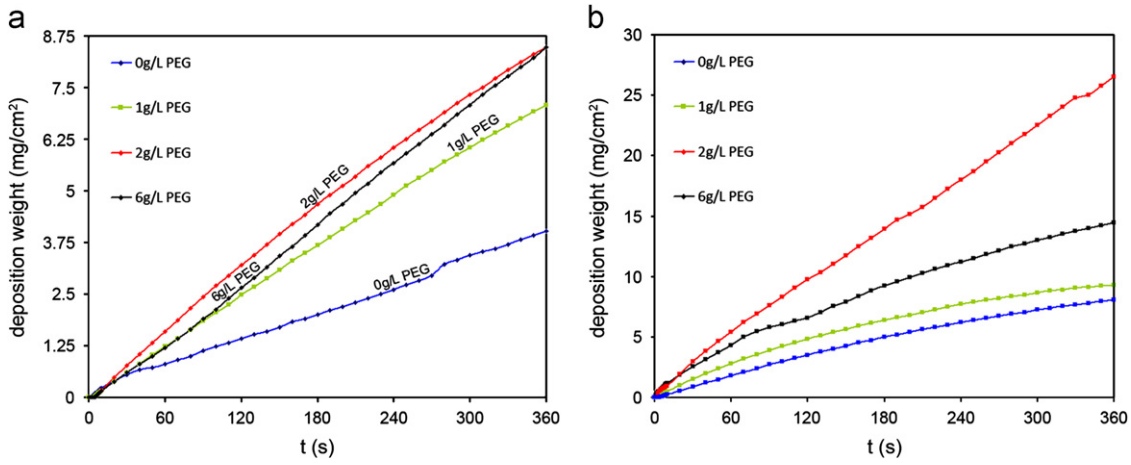

Fig. 8. Immersion weight of deposits against time at (a) 60 and (b) 200 V from the suspensions with the different concentrations of PEG.

current density decreases and the resistance increases more steeply with time due to the faster deposition at higher voltage (so the thicker deposit at same time). As can be seen the current density increases at both voltages with increase in the PEG concentration, due to an enhancement in the suspension conductivity with PEG concentration (Fig. 3). Because of the very high resistivity of HA nanoparticles, the resistance of deposit and suspension is nearly equal to that of the liquid phase present between the particles in them (interparticles liquid). The resistance of suspension (and so interparticles liquid) decreases with PEG concentration (Fig. 3) resulting in the resistance reduction with PEG concentration. As explained previously at 2 g/L PEG the surface of HA nanoparticles are saturated by H^+PEG resulting in the maximum zeta potential for them; so at this concentration the voltage drop over the deposit ($R_{d,t}$ i_t) is the minimum (since the deposit resistance and the current passing through the circuit are the minimum) resulting in the maximum value of effective field over the suspension (Eq. (4)). Similar results and discussion have been reported

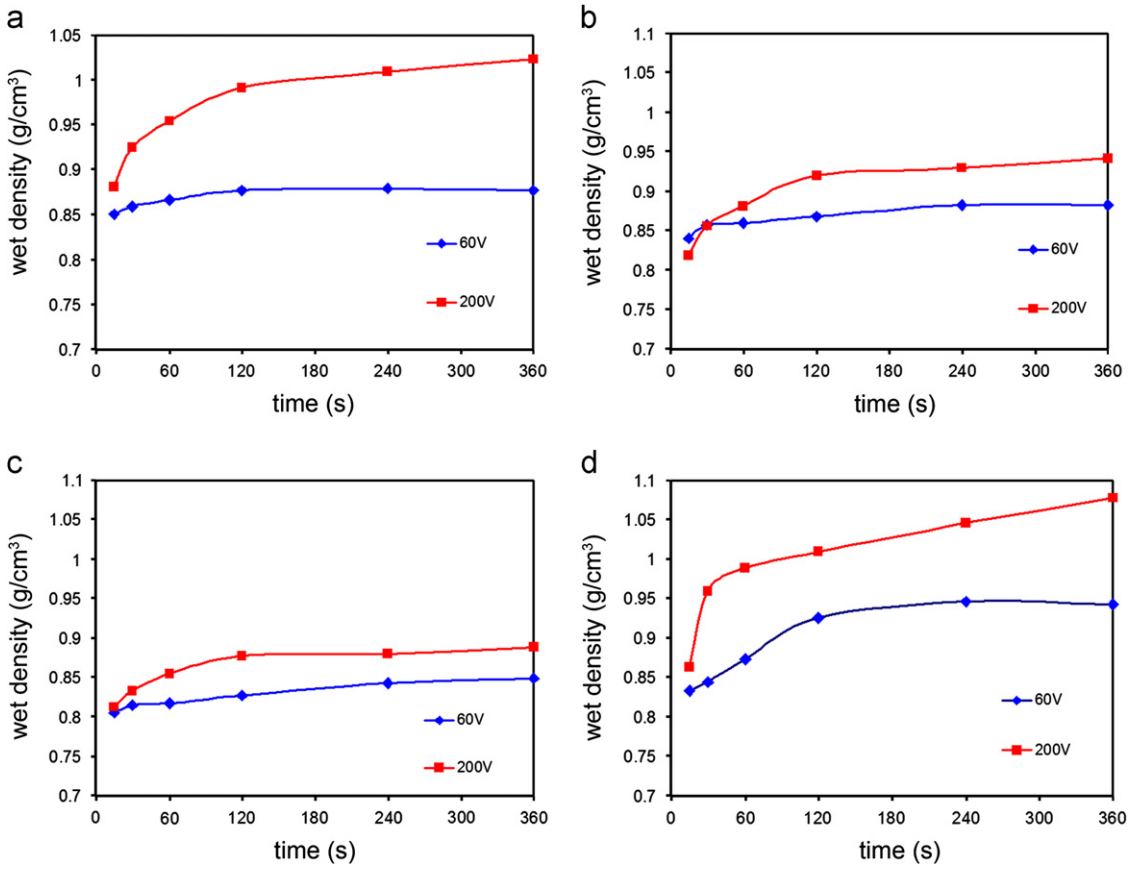

Fig. 9. Wet density of deposits against time at (a) 60 and (b) 200 V from the suspensions with different concentrations of PEG.

for the EPD of titania nanoparticles in isopropanol with triethanolamine as an additive [32].

3.3.2. Deposition kinetic

The immersion weight of deposits against time at 60 and 200 V from the suspensions with different concentrations of PEG is shown in Fig. 8. As can be seen in all cases the deposition weight increases with deposition voltage and time in agreement with Eq. (1). At both voltages and at same deposition time the deposition rate is the fastest than the suspension with 2 g/L PEG, due to the higher zeta potential (so the higher mobility according to Eq. (2)) of HA nanoparticles in it (Fig. 4). The deposition rate decreases with time (deviation from linearity) due to the voltage drop over the deposit (with high resistivity) as well as the depletion of suspension from the particles. Also the decline in deposition rate is higher at 200 V, due to the higher voltage drop over the deposit (since the thicker the deposit, the higher the resistance of it) as well as more depletion of suspension from particles. Also it can be seen that the deviation from linearity is the highest for the suspension with 0 g/L PEG (due to the lowest effective field across the suspension due to the very high $R_{d,t}$, Fig. 7) and the lowest for the suspension with 2 g/L PEG (due to the highest effective field across the suspension, Fig. 7).

3.3.3. Wet density of deposits

The wet density of deposits formed at 60 and 200 V from the suspensions with different concentrations of PEG against EPD time is shown in Fig. 9. As can be seen the wet density of deposits from all suspensions increases with deposition time at both voltages. Also at the same deposition time the wet density is higher at 200 V than at 60 V. The increase in wet density with time is caused by particles rearangement within the deposit during EPD due to the electro-osmotic flow around them [35,36]. Particles rerangement needs time to occur so the wet density increases with EPD time. Also the electro-osmotic flow is more intensive at higher votages [39,40], so the wet density is higher at larger applied voltage.

3.3.4. Microstructure of deposits

The SEM images of the coatings deposited at 60 V (same deposition weight) from the suspensions with the different concentrations of PEG are shown in Fig. 10. As can be seen in the SEM images of unsintered coatings, the coating deposited from the suspension with 2 g/L PEG has a finer microstructure with fewer agglomereates than those deposited from other suspensions due to the higher zeta potential of HA nanoparticles in it. The higher the zeta potential, the higher the electrostatic repulsion force between particles, resulting in less agglomeration. During

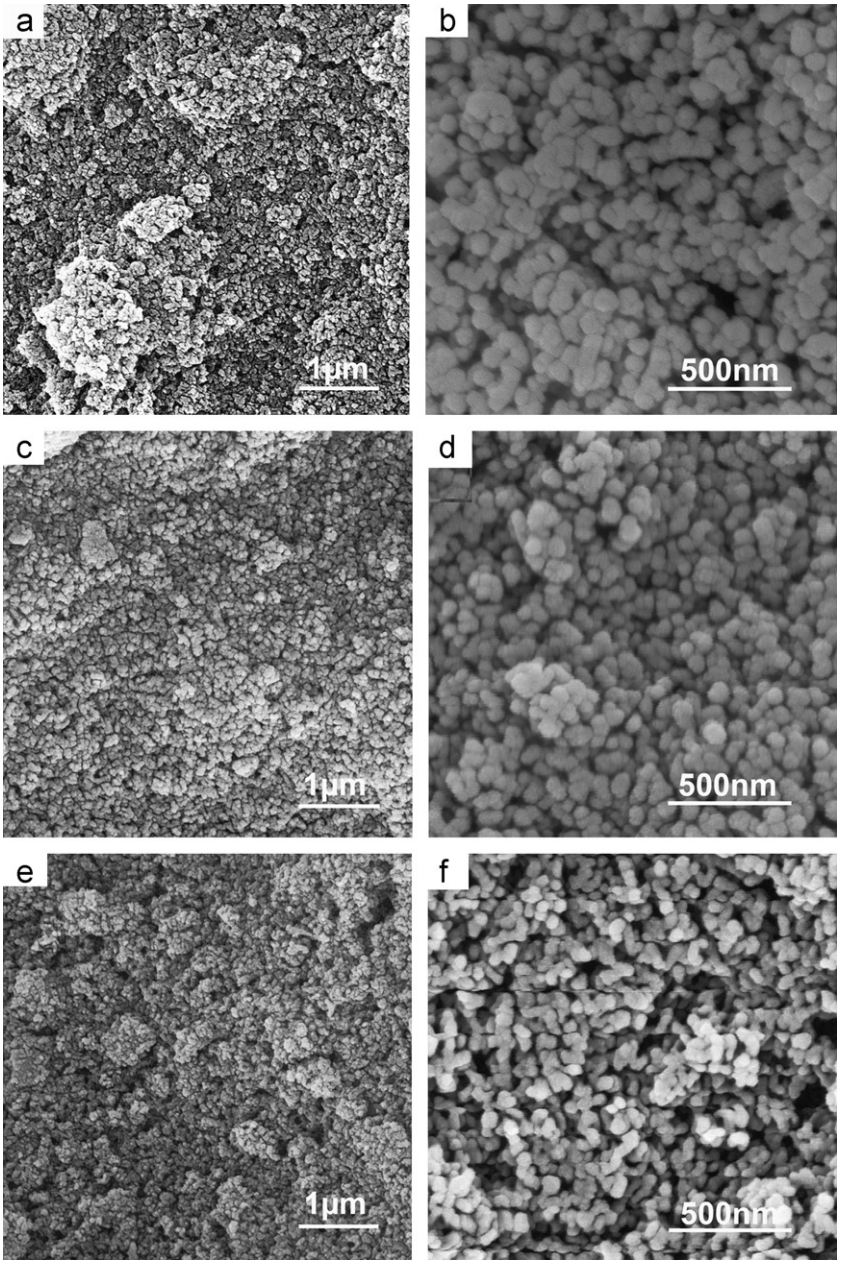

Fig. 10. SEM images of the coating deposited from the suspensions with (a,b) 0, (c,d) 2 and (e,f) 6 g/L PEG (a,c,e) befor and (b,d,f) after sintering.

EPD, the agglomerated particles can also migrate toward the electrode with opposite charge and deposit on it. As can be seen in the SEM images of sintered coatings (Fig. 10(b,d,f)) the coatings deposited from the suspension with 0 and 6 g/L PEG are more porous than that deposited from the one with 2 g/L PEG; this is due to agglomerated micostructure of these coatings in green state resulting in their poor sinterability. In adition to this, the burn out of PEG adsorbed on HA nanoparticles during sintering can also result in porous microstructure of coatings deposited from the suspension with 6 g/L PEG. As can be seen in Fig. 11 the coatings deposited from the suspensions with PEG additive have fewer cracks so that no crack can be seen in those deposited from the ones with 2 and 6 g/L PEG; however some cracks are still present in the coating deposited from the suspension with 1 g/L PEG. PEG acts as a binder in the deposits and sticks the particles together in it to prevent from cracking. When the concentration of PEG in the suspension is higher than 2 g/L, its amount is enough to strongly stick all particles together in the deposit.

3.3.5. *Corrosion resistance of coating*

The polarization plot for the deposits formed from the suspensions with the different concentrations of PEG in Ringer's solution is shown in Fig. 12. As can be seen all coatings increase the corrosion resistance of substrate proving that HA coatings act as a good barrier layer

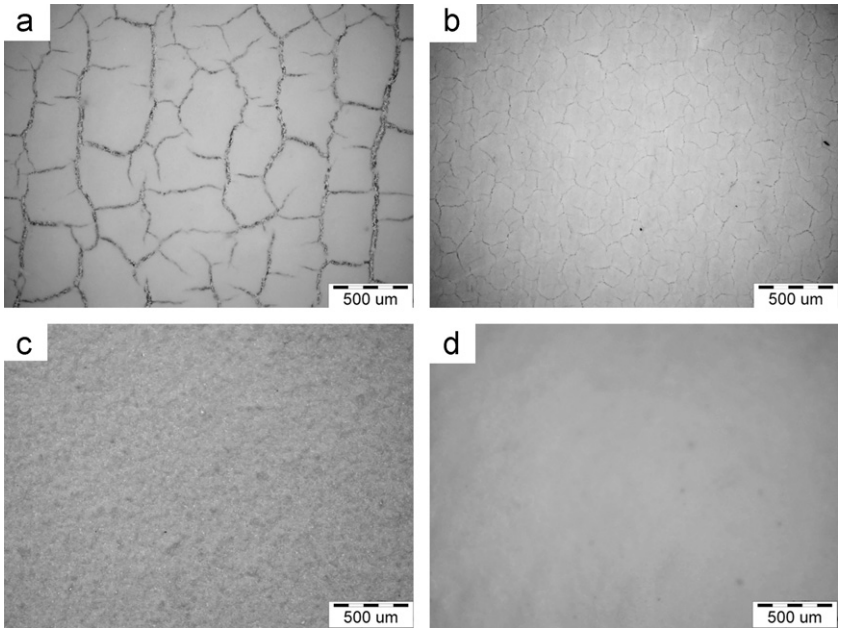

Fig. 11. Optical images of the coating deposited at 60 V (same weight) from the suspensions with (a) 0, (b) 1, (c) 2 and (d) 6 g/L PEG.

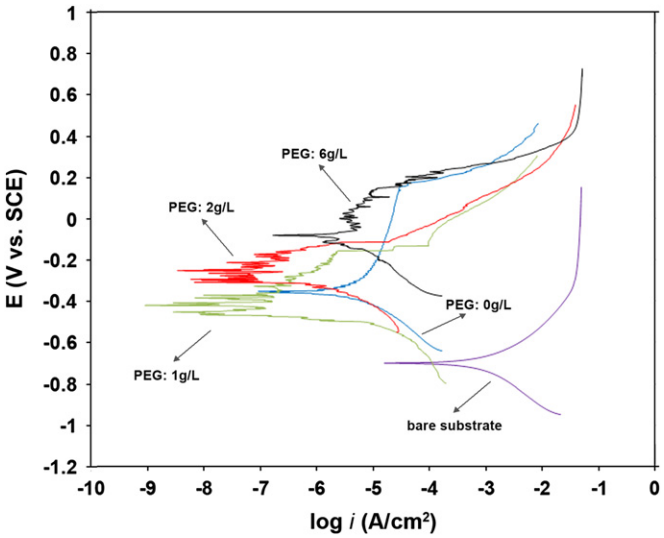

Fig. 12. Corrosion resistance of the deposits formed at 60 V from the suspensions with different concentrations of PEG.

between substrate and corrosive fluid. It can be seen that the coatings deposited from the suspensions with PEG additive have more corrosion resistance than that deposited from the one without PEG; as explained previously PEG in the coatings acts as a binder and prevent their cracking; as expected the coating deposited from the suspension with 2 g/L PEG has the highest corrosion resistance, since this coating has a dense and homogeneous microstructure (Fig. 10(d)) without cracking (Fig. 11(c)). The coating deposited from the suspension with 6 g/L PEG has the lower corrosion resistance than that deposited from the one with 2 g/L PEG, while both deposits have no cracks in their microstructure; this is due to the porous microstructure of the coatings deposited from the suspension with 6 g/L PEG (Fig. 10(f)) allowing the corrosive fluid to penetrate toward the substrate surface through the pores and corrode it.

4. Conclusion

The suspensions of HA nanoparticles in isopropanol were prepared and polyethylene glycol (PEG) was used as the dispersant. It was found that PEG is protonated in isopropanol and then adsorbed on the HA nanoparticles surfaces increasing their stability by an electrosteric stabilization mechanism. The zeta potential of particles was the highest at the PEG concentration of 2 g/L. It was found that the effective electric field over the suspension is the highest for the suspension with 2 g/L PEG. The deposition rate is the fastest from the suspension with 2 g/L PEG due to the highest zeta potential (so the higher mobility) of HA nanoparticles in it. The wet density of deposits increases with deposition time and voltage due to electro-osmotic flow in deposit. It was observed that the microstructure of the deposit formed from the suspension with 2 g/L PEG is finer with less agglomeration than others. Also this coating has the most corrosion resistance. So it can be concluded that the optimum dosage of PEG is 2 g/L in the 10 g/L suspension of HA nanoparticles in isopropanol.

References

[1] D.H. Kohn, Metals in medical application, Current Opinion in Solid State and Material Science 3 (1998) 309–316.
[2] V.K. Balla, S. Bodhak, S. Bose, A. Bandyopadhyay, Porous tantalum structures for bone implants: fabrication, mechanical and in vitro biological properties, Acta Biomaterialia 6 (2010) 3349–3359.

[3] R.M. Pilliar, Porous-surfaced metallic implants for orthopedic applications, Journal of Biomedical Materials Research 21 (1987) 1–33.
[4] E. Marin, S. Fusi, M. Pressacco, L. Paussa, L. Fedrizzi, Characterization of cellular solids in Ti_6Al_4V for orthopedic implant applications: trabecular titanium, Journal of the Mechanical Behaviour of Biomedical Materials 3 (2010) 373–381.
[5] M. Pourbaix, Electrochemical corrosion of metallic biomaterials, Biomaterials 5 (1984) 122–134.
[6] F.W. Sunderman, Carcinogenicity of metal alloys in orthopedic prostheses: clinical and experimental studies, Journal of the Mechanical Behaviour of Biomedical Materials 13 (1989) 205–216.
[7] M.A. Mcgee, D.W. Howie, K. Costi, D.R. Haynes, C.I. Wildenauer, M.J. Pearcy, J.K. Mclean, Implant retrieval studies of the wear and loosening of prosthetic joints: a review, Wear 241 (2000) 158–165.
[8] L.M. Rabbe, J. Rieu, A. Lopez, P. Combrade, Fretting deterioration of orthopedic implant materials: search for solution, Clinical Materials 15 (1994) 221–226.
[9] D.W. Hoeppner, V. Chandrasekaran, Fretting in orthopedic implants: a review, Wear 173 (1994) 187–189.
[10] Y. Ramaswamy, C.T. Wu, H. Zreiqat, Orthopedic coating materials: considerations and applications, Expert Review of Medical Devices 6 (2009) 423–430.
[11] S.R. Paital, N.B. Dahotre, Calcium phosphate coatings for bio-implant applications: materials, performance factors, and methodologies, Materials Science and Engineering R 66 (2009) 1–70.
[12] M. Sygnatowicz, A. Tiwari, Controlled synthesis of hydroxyapatite-based coatings for biomedical application, Materials Science and Engineering C 29 (2009) 1071–1076.
[13] M.H. Fathi, A. Doostmohammadi, Bioactive glass nanopowder and bioglass coating for biocompatibility improvement of metallic implant, Journal of Materials Processing Technology 209 (2009) 1385–1391.
[14] M. Wei, A.J. Ruys, B.K. Milthorpe, C.C. Sorrell, Precipitation of hydroxyapatite nanoparticles: effects of precipitation method on electrophoretic deposition, Journal of Materials Science Materials in Medicine 16 (2005) 319–324.
[15] P. Wang, C. Li, H. Gong, X. Jiang, H. Wang, K. Li, Effects of synthesis conditions on the morphology of hydroxyapatite nanoparticles produced by wet chemical process, Powder Technology 203 (2010) 315–321.
[16] X. Pang, I. Zhitomirsky, Electrodeposition of composite hydroxyapatite–chitosan films, Materials Chemistry and Physics 94 (2005) 245–251.
[17] Xiu Feng Xiao, Rong Fang Liu, Effect of suspension stability on electrophoretic deposition of hydroxyapatite coatings, Matrials Letters 60 (2006) 2627–2632.
[18] D.M. Liu, Q. Yang, T. Troczynski, Sol–gel hydroxyapatite coatings on stainless steel substrates, Biomaterials 23 (2002) 691–698.
[19] S. Dyshlovenko, L. Pawlowski, B. Pateyron, I. Smurov, J.H. Harding, Modelling of plasma particle interactions and coating growth for plasma spraying of hydroxyapatite, Surface and Coatings Technology 200 (2006) 3757–3769.
[20] B. Mavis, A.C. Taş, Dip coating of calcium hydroxyapatite on Ti–6Al–4V substrates, Journal of the American Ceramic Society 83 (2000) 989–991.
[21] J. Long, L. Sim, S. Xu, K. Ostrikov, Reactive plasma-aided RF sputtering deposition of hydroxyapatite bio-implant coatings, Chemical Vapour Deposition 13 (2007) 299–306.
[22] C.F. Koch, S. Johnson, D. Kumar, M. Jelinek, D.B. Chrisey, A. Doraiswamy, C. Jin, R.J. Narayan, I.N. Mihailescu, Pulsed laser deposition of hydroxyapatite thin films, Materials Science and Engineering C 27 (2007) 484–494.
[23] I. Zhitomirsky, L. Gal-Or, Electrophoretic deposition of hydroxyapatite, Journal of Materials Science: Materials in Medicine 8 (1997) 213–219.
[24] J. Ma, C. Wang, K.W. Peng, Electrophoretic deposition of porous hydroxyapatite scaffold, Biomaterials 24 (2003) 3505–3510.
[25] J. Ma, C.H. Liang, L.B. Kong, C. Wang, Colloidal characterization and electrophoretic deposition of hydroxyapatite on titanium substrate, Journal of Materials Science: Materials in Medicine 14 (2003) 797–801.
[26] L. Besra, M. Liu, A review on fundamentals and applications of electrophoretic deposition (EPD), Progress in Materials Science 52 (2007) 1–61.
[27] S.D. Cook, K.A. Thomas, J.E. Delton, T.K. Volkman, S. Whitecloud III, J.F. Key, Hydroxylapatite coating of porous implants improves bone ingrowth and interface attachment strength, Journal of Biomedical Materials Research 26 (1992) 989–1001.
[28] H.C. Hamaker, Formation of a deposit by electrophoresis, Transactions of the Faraday Society 35 (1940) 279–287.
[29] M. von Smoluchowski, Versuch einer mathematischen theorie der koagulationkinetik kolloider loesungen, Zeitschrift für Physikalische Chemie 92 (1917) 129–132.
[30] T. Uchikoshi, K. Ozawa, B.D. Hatton, Y. Sakka, Electrophoretic deposition of alumina suspension in a strong magnetic field, Journal of Materials Research 16 (2) (2001) 321–324.
[31] M. Farrokhi-Rad, M. Ghorbani, Electrophoretic deposition of titania nanoparticles in different alcohols: kinetics of deposition, Journal of the American Ceramic Society 94 (2011) 2354–2361.
[32] M. Farrokhi-Rad, T. Shahrabi, Electrophoretic deposition of titania nanoparticles: sticking parameter determination by an in-situ study of the EPD kinetics, Journal of the American Ceramic Society 95 (2012) 3434–3440.
[33] R. Damodaran, B.M. Moudgil, Electrophoretic deposition of calcium phosphates from non-aqueous media, Colloids and Surfaces A: Physicochemical and Engineering Aspects 80 (1993) 191–195.
[34] S.G.J. Heijman, H.N. Stein, Electrostatic and sterical stabilization of TiO_2 dispersions, Langmuir 11 (1995) 422–427.
[35] L. Saravanan, S. Subramanian, A.V. Kumar, R.N. Tharanathan, Surface chemical studies on SiC suspension in the presence of chitosan, Ceramics International 32 (2006) 637–646.
[36] C. Lau, Y. Mi, A study of blending and complexation of poly (acrylic acid)/poly (vinyl pyrrolidone), Polymer 43 (2002) 823–829.
[37] T. Ishikawa, Surface structure and molecular adsorption of apatites, Studies in Surface Science and Catalysis 99 (1996) 301–318.
[38] H. Tanaka, T. Watanabe, M. Chikazawa, FTIR and TPD studies on the adsorption of pyridine, n-butylamine and acetic acid on calcium hydroxyapatite, Journal of the Chemical Society, Faraday Transactions 93 (24) (1997) 4377–4381.
[39] Y. Solomentsev, M. Bohmer, J.L. Anderson, Particle clustering and pattern formation during electrophoretic deposition: a hydrodynamic model, Langmuir 13 (1997) 6058–6068.
[40] C.H. Ji, W. Lan, P. Xiao, Fabrication of yttria-stabilized zirconia coatings using electrophoretic deposition: packing mechanism during deposition, Journal of the American Ceramic Society 91 (2008) 1102–1109.